*Int. J. Electrochem. Sci.*, 12 **(2017)** 8820 – 8831, doi: 10.20964/2017.09.08

International Journal of
ELECTROCHEMICAL
SCIENCE
www.electrochemsci.org

# Direct Formation of Reduced Graphene Oxide and Graphene Quantum dot Composites by Using Ascorbic Acid as High-Performance Binder-Free Supercapacitor Electrodes

*Yongjie Xu, Yukun Feng, Xinyu Li*[*]*, Guanghui Hu, Yi Luo, Lang Sun, Tao Tang, Jianfeng Wen, Heng Wang, and Ming Li*[*]

College of Science & Ministry-province jointly-constructed cultivation base for state key laboratory of Processing for mom-ferrous metal and featured materials & Key Lab. of Nonferrous Materials and New Processing Technology, Guilin University of Technology, Guilin 541004, China.
[*]E-mail: lixinyu5260@163.com, liming928@163.com
Yongjie Xu and Yukun Feng contributed equally to this work.

*Received:* 25 May 2017 / *Accepted:* 29 June 2017 / *Published:* 13 August 2017

With unique structural features and hydrophilic functional groups, graphene quantum dots (GQDs) and graphene oxide (GO) are potential materials for supercapacitor electrodes. In this work, GQDs decorated with a GO hybrid and an interconnected nickel network are successfully fabricated and subjected to reduction treatment with ascorbic acid. GO and GQD composites (GO/GQDs) exhibit with different mass ratios of GO to GQDs (6:1, 3:1, 1:1) are also investigated. The specific capacitance (Csp) of the reduced GO (rGO)/GQD composites is higher than that of rGO. Among the composites with different mass ratios, the rGO/GQD composites with GO:GQDs=3:1 exhibit the highest electrochemical performance because the intercalation of GQDs into GO nanosheets can promote electron transportation and thus reduce the internal resistance and charge transfer resistance of the electrode. Additionally, the GQDs with large specific surface area can enhance the interfacial property among GO. It yields a Csp of 296 F $g^{-1}$ at a current density of 0.5 A $g^{-1}$ and 85% retention after 3,000 cycles of charge/discharge. Csp remarkably decreases when the mass ratio of GO to GQDs increases to 1:1 possibly because of blocked ion channels from a large amount of GQDs loaded on the GO surface.

**Keywords:** Graphene oxide quantum dots, Graphene oxide, Reduction, Supercapacitors, Composites

## 1. INTRODUCTION

With rapid global economical development, tremendous research has focused on competent, sustainable, and clean sources of energy conversion and storage. Supercapacitors have received

increasing attention because of their longer cycle-life, higher power density, and more safty compare to lithium-ion battery.[1-7] Graphene-based materials are promising components for supercapacitors because of their unique electrical, chemical, and physical properties, such as high electrical conductivity and large surface area.[8-10] Pure carbon-based supercapacitors usually store charge through an electrochemical double-layer effect on an electrode surface.[11] For this application, reduced graphene oxide (rGO) nanosheets have been widely investigated because they can be cheaply produced from graphene oxides (GO) in a large scale. However, the intrinsic capacitance of as-prepared highly rGO is ≤100 F/g, which is below the expected theoretical value of 550 F/g.[12, 13] In practice, GO is directly used as a starting material, but the specific capacitance of graphene has been limited because of its restacking[14, 15] that inhibits electrolyte diffusion and decreases the surface area; as a result, supercapacitor performance is compromised.[16]

To explore the full potential of GO and enhance the electrochemical performance of graphene electrodes, we should place a spacer between chemically derived graphene sheets and thus minimize stacking and maximize the specific surface area.[17,18] "Stabilizers" or "spacers" have also been incorporated into graphene layers to inhibit the agglomeration of reduced graphene sheets. Wallace[19] proposed the use of polypyrrole (PPy) nanoparticles as spacers between graphene layers to generate free-standing films with high mechanical properties and large capacitance per area. Fan[20] prepared graphene or carbon black composites through ultrasonication and in-situ reduction of GO. As spacers, carbon black particles can inhibit graphene sheet agglomeration and consequently improve electrolyte–electrode accessibility. To an extent, energy density can be enhanced by incorporating pseudocapacitive materials, such as metal oxide nanoparticles, including $RuO_2$, $MnO_2$, $Fe_2O_3$, and $NiO_x$.[21-25] However, the high electrical resistance of transition metal oxides causes a poor rate capability, and pseudocapacitive materials commonly exhibit poor stability and high resistance during charge/discharge process because of their relatively poor structural stability, active material loss, or excessive oxidative decomposition.[26]

Since the discovery of new generations of graphene quantum dots (GQDs) with tunable properties, the range of applications involving carbon materials has been extended.[27,28] GQDs are known as zero-dimensional nanomaterials with single- or few-layer graphene particles, and these structures effectively prevent restacking.[29] Dispersibility in various solvents, large open surfaces, and free edges have also been considered in the design of supercapacitors with high specific capacitances because of their high electron mobility.[30] The electrochemical capacitive properties of GQDs and their applications in GQD micro-supercapacitors[31] and GQD/graphene supercapacitors[32-34] have shown that GQDs can considerably improve the performance of supercapacitors. Therefore, we expected that GQDs deposited on a graphene electrode can improve the specific surface areas (SSA) of electrode materials and simultaneously create additional micropores that would significantly contribute to the overall electrochemical capacitance because of the small size of GQDs.[35] Despite the superior characteristics of GQDs as active materials of supercapacitors, the combined bulk graphene and GQD materials or films have been rarely reported. Unfortunately, GQDs are also seldom applied to enhance the capacitive property of the GO matrix significantly. Therefore, theoretical and practical studies should determine whether basic carbon building blocks, such as GQDs, can be utilized to construct highly capacitive carbon frameworks. However, the above

materials used for supercapacitor electrodes show different electrochemical performance due to different preparation and reduction methods.[36-41]

In this study, GO was used as a graphene precursor to construct high-performance supercapacitors by utilizing well-functionalized single-crystalline GQDs with rich redox sites. GO can be easily dispersed in water because of its hydrophilic groups, such as carboxyl and carbonyl groups, attached on surfaces and edges.[42] GO can serve as a surfactant to disperse GQDs in water and consequently form GO/GQD suspension in the fabrication of electrodes. Once dried, GO can simultaneously form a membrane. As such, a binder is unnecessary to fabricate electrodes. To enhance conductivity and capacitance, we reduced the GO/GQD composites with ascorbic acid and investigated the composites with different mass ratios of GO to GQDs (6:1, 3:1, 1:1). The rGO/GQD-3:1 can deliver an ultrahigh specific capacitance of 296 F $g^{-1}$ at a current density of 0.5 A $g^{-1}$ and 85% capacity retention after 3,000 charge/discharge cycles. The resulting GQDs among the graphene sheets enlarge the interlayer spacing of graphene and prevent their agglomeration. The enlarged interlayer distance also enables the rapid transfer of electrolyte ions throughout the electrode material to improve the capacitance performance of this material.

## 2. EXPERIMENTAL

### *2.1 Preparation of materials*

GO was prepared by a modified Hummers' method. GQDs was purchased from Nanjing JI Cang Nano Technoloyg Co., Ltd., China. Ni foam sheets（with a size of 2.5 cm × 1 cm × 0.1 cm） were carefully cleaned in hydrochloric acid to etch the surface oxide layer and remove contaminants, then was immersed in acetone to remove organic materials from the surface. Finally, it was washed with deionized water and absolute ethanol to make the Ni foam sheets more hydrophilic. A well-dispersed aqueous solution of GO was prepared by putting 30 mg of GO in 2 ml of deionized water by ultrasonication for 2 hours to open the layers of GO. Then the GO solution was mixed with GQDs (the mass of GO and GQDs in the rate of 6:1, 3:1, and 1:1) and stirred 5min. After that, the mixture was sonicated for 1 hour for the attachment of GQDs onto GO layers.

### *2.2 Synthesis of rGO/GQDs electrodes*

The nickel foam sheets were firstly immersed into a GO/GQDs dispersion to ensure that GO/GQDs were filled into the microspores of Ni foam, and then dried for few hours in room temperature. Then the mixture was coated on nickel foam and dried for few hours in room temperature to remove the water. This step was repeated a number of times to increase the GO/GQDs loading. The nickel foam sheet coated with GO/GQDs was transferred to ascorbic acid aqueous solution (10 mg $ml^{-1}$) and maintained at 60 ℃ in a water bath for 5 hours. They were repeatedly rinsed with deionized water and dried for use. The synthesis scheme was illustrated in Fig. 1.

*2.3 Characterization*

The morphological and microstructural details of the samples were examined by a field emission scanning electron microscopy (FE-SEM, S-4800) and transmission electron microscopy (TEM, JEM-2100F). The data of XPS were recorded on ESCALAB 250Xi to confirm the chemical bonding nature of the composite material.

*2.4 Electrochemical Testing*

The electrochemical performance of the GO/GQD electrodes were performed by cyclic voltammetry (CV), galvanostatic charge-discharge (GCD) and electrochemical impendence spectroscopy (EIS) in a two-electrode system using a CHI760E electrochemical workstation. Two identical electrodes were separated by a separator (NKK TF45, 40 μm). An aqueous solution of 6 M KOH was used as the electrolytes.

Specific capacitances $C_s$ (F $g^{-1}$) can be calculated from the discharge processes using the following formula:

$$C_s = \frac{4I\Delta t}{m\Delta V} \quad (1)$$

where I is the discharge current (A), Δt is the discharge time (s), m is the total mass of both electrodes (g), and ΔV is the voltage range (V).

Energy and power density are two important parameters for measuring the practical application of as-made supercapacitors. The energy density E (Wh $kg^{-1}$) and power density P (W $kg^{-1}$) of the symmetric supercapacitors were calculated by charge/discharge curves based on the following formulas:

$$E = \frac{C_s}{8}\Delta V^2 \frac{1}{3.6} \quad (2)$$

$$P = \frac{E}{\Delta t} \quad (3)$$

Where Δt is the discharge time (h).

## 3. RESULTS AND DISCUSSION

*3.1 Characterization of rGO/GQD composites*

The morphological characteristics and nanostructures of the as-synthesized graphene-based materials are described through scanning electron microscopy (SEM) and transmission electron microscopy (TEM). The results are presented in Fig. 1. It is seen that rGO is consisted of several layers of interconnected graphene sheets with a prominently crumpled and wrinkled nanosheets morphology (Fig. 1b), which is derived from the high-oxygen-containing groups on the surface of GO tightly bound to residual $H_2O$ molecules.[43] In the TEM image of GQDs (Fig. 1c), uniform GQDs with sizes of less than 10 nm are observed.

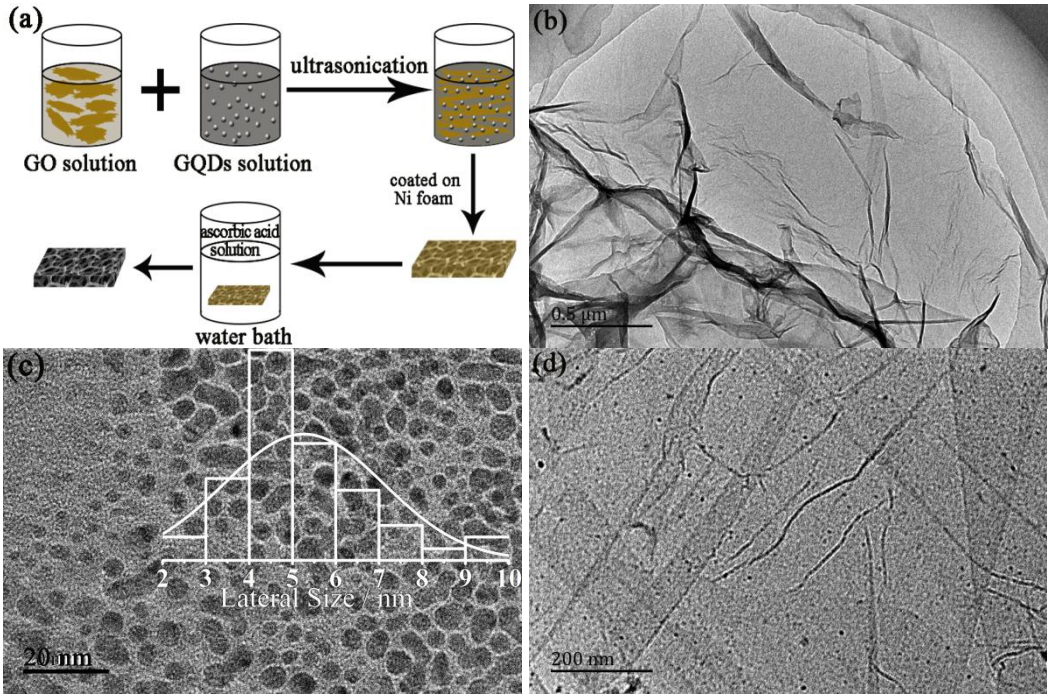


**Figure 1**. (a) Schematic diagram of the process for fabricating electrodes. (b)-(d) TEM images of GO, GQDs and rGO/GQDs-(3:1).

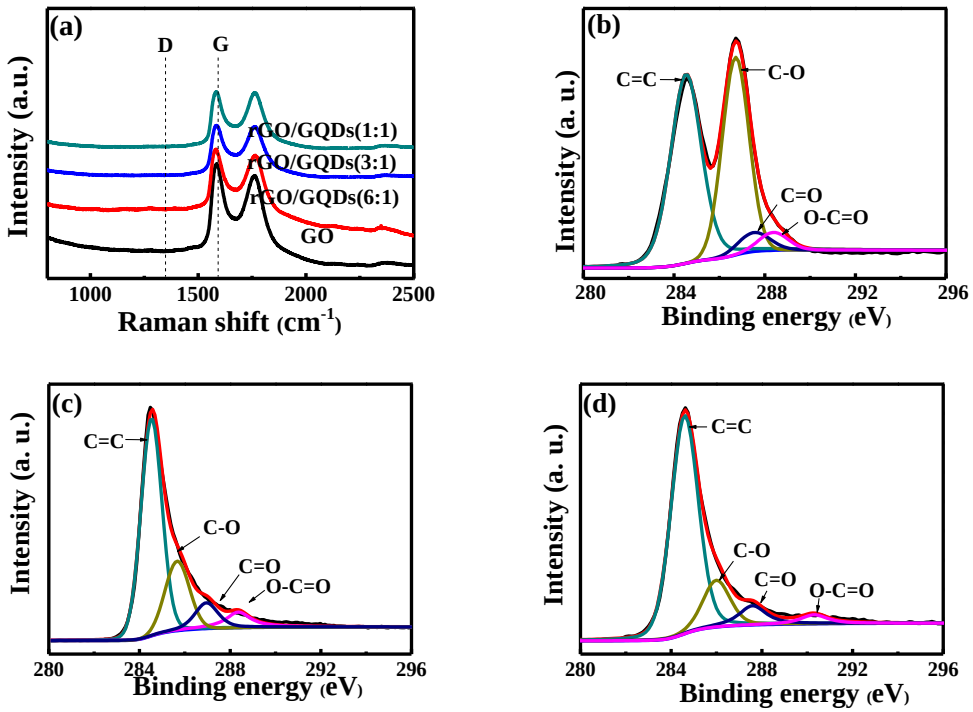


**Figure 2.** (a) Raman spectra of GO, rGO/GQDs-6:1, rGO/GQDs-3:1, and rGO/GQDs-1:1. (b), (c) and (d) High resolution C1s XPS spectra of GO, rGO and rGO/GQDs-3:1.

Figure 1d shows GQDs anchored on GO nanosheets. GQD and GO suspensions are mixed through ultrasonication, while GQDs are directly anchored on the hydrophilic surface of the GO sheets

through covalent chemical bonding and van der Waals force. GQDs can prevent the aggregation of GO nanosheets and thus increase the number of ion channels in the interior of materials.[44]

The defective nature of the samples is reflected in the Raman spectra. In Fig. 2a, all of the samples possess two main peaks, which are assigned to D band at approximately 1349 $cm^{-1}$ attributed to the structural defects of carbon and G band at around 1594 $cm^{-1}$ ascribed to the in-plane vibrations of $sp^2$ carbon atoms.[45] The $I_D/I_G$ ratio of GO is 0.88, which indicates a relatively low graphitized GO because of the presence of oxygen-containing functional groups. Compared with the $I_D/I_G$ ratio of GO, the increased $I_D/I_G$ ratio of rGO (1.02) demonstrates the formation of structural defects after GO is electrochemically reduced. The introduced defects can significantly increase the surface area of graphene and thus improve supercapacitive performance of the activated graphene. In addition, the $I_D/I_G$ ratio of rGO/GQD-3:1 composite is 1.06, which is slightly higher than that of rGO (1.02). This finding clearly suggests that the loading GQDs on the GO sheets can increase the number of defects or edges and the randomness of graphene sheets.

The surface chemical identification of GO, rGO, and rGO/GQD-3:1 is performed through X-ray photoelectron spectroscopy. Figures 2b, c, and d illustrate the high-resolution C 1*s* spectra of GO, rGO, and rGO/GQD-3:1, respectively. The spectrum of GO can be deconvoluted into four peaks located at approximately 284.6, 286.7, 287.6, and 288.4 eV that correspond to $sp^2$-hybridized graphitic carbon (C=C), carbon in C–O bonds, carbonyl carbon (C=O), and carboxyl carbon (O–C=O), respectively. After reduction reaction and carbonization are facilitated by ascorbic acid aqueous solution, the oxygen-containing functional groups are reduced significantly.[46] The proportion of C=C peak of rGO/GQD-3:1 is higher and its percent values of C=O, C−O, and O−C=O peaks are lower than those of pure rGO. The reduction effect is greatly improved because of the addition of GQDs.

### *3.2 Electrochemical performance of rGO/GQDs*

Two electrode symmetric supercapacitors are assembled to demonstrate the performance of three samples as supercapacitor (ultracapacitor) electrodes. Their electrochemical performances are characterized by cyclic voltammetry (CV), galvanostatic charge-discharge (GCD), and electrochemical impedance spectroscopy (EIS) in an aqueous solution of 6 M KOH with the potential range of 0–1 V to avoid pseudocapacitance increase or capacitance decay.[30, 47] The CV curves of the as-prepared electrode materials at the scan rates of 10, 50, and 100 mV $s^{-1}$ (Figures 3a–c) are relatively rectangular without visible distortion, and this observation indicates an ideal capacitance behavior. The integrated areas of the CV curves of rGO/GQD-3:1 are larger than those of the other samples, and this finding demonstrates that the specific capacitance of rGO/GQD-3:1 is higher than that of the other composites probably because of the formation of the continuous film-like structure of the conductive GQDs.[48] GQDs can be effectively used to prevent the restacking of graphene and provide additional surface active sites and accessible edges.[16, 49] Moreover, the deposition of GQDs on GO nanosheets likely enhances the specific surface area of rGO electrodes and create additional micropores that possibly contribute to the overall electrochemical capacitance because of the small size of GQDs. GQDs are

composed of abundant functional groups that can repair GO defects when GQDs are anchored on the surface of GO. The area surrounded by the CV curves of rGO/GQD-1:1 is the smallest among the observed areas, and this finding implies that large amounts of GQDs are loaded on the GO surface and consequently form an electrolyte ion block; thus, the sample possesses less pore volume.[50] The electrode surface is blocked, and it subsequently exhibits slow heterogeneous electron transfer kinetics because of the low edge/basal plane ratio; in addition, poor electrochemical performance is observed.[51] In Figure 3d, the CV curves of the rGO/GQD-3:1 symmetric supercapacitor maintain a typical rectangular form when the scan rate increases from 5 mV $s^{-1}$ to 200 mV $s^{-1}$, and this result suggests a low equivalent series resistance and an ideal capacitive behavior.

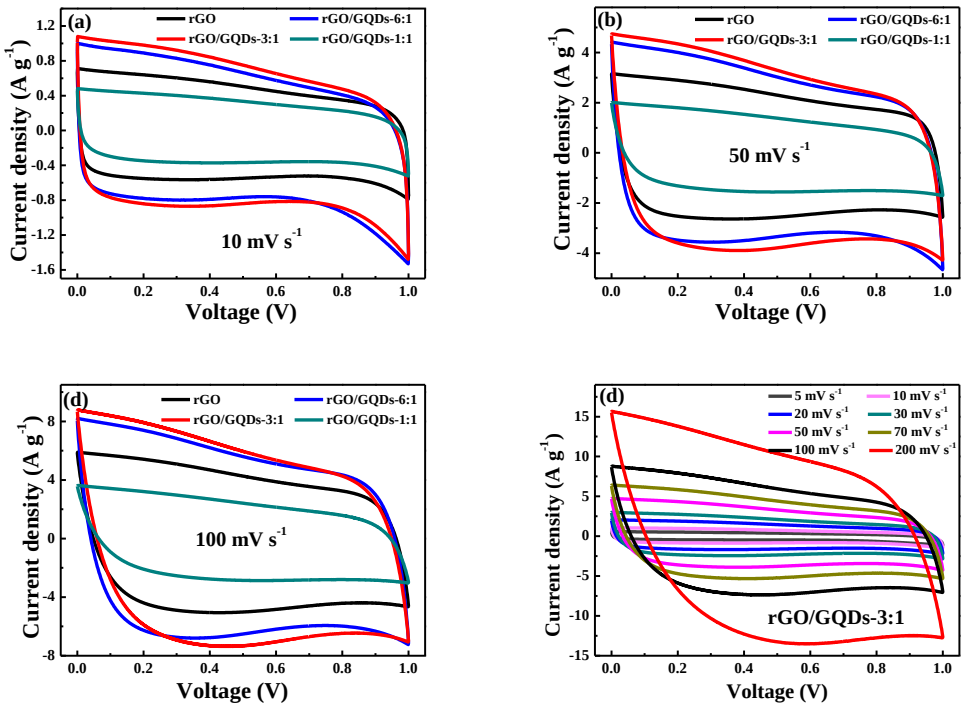


**Figure 3.** (a)-(c) CV curves of four electrodes at scan rates of 10 mV $s^{-1}$, 50 mV $s^{-1}$, and 100 mV $s^{-1}$. (d) CV curves of rGO/GQDs-3:1 electrode at different scan rates in 6 M KOH.

The GCD curves of the samples at current densities of 0.5, 1, and 2 A $g^{-1}$ are shown in Figs. 4a–c. These data are consistent with the CV curves, and the capacitance performance of rGO/GQD-3:1 is superior to those of rGO and other composites. Figure 4d shows the GCD curves of rGO/GQD-3:1 at different current densities ranging from 0.5 A $g^{-1}$ to 10 A $g^{-1}$. All of the curves are generally linear and symmetrical, which suggests excellent capacitive performance and electrochemical reversibility.

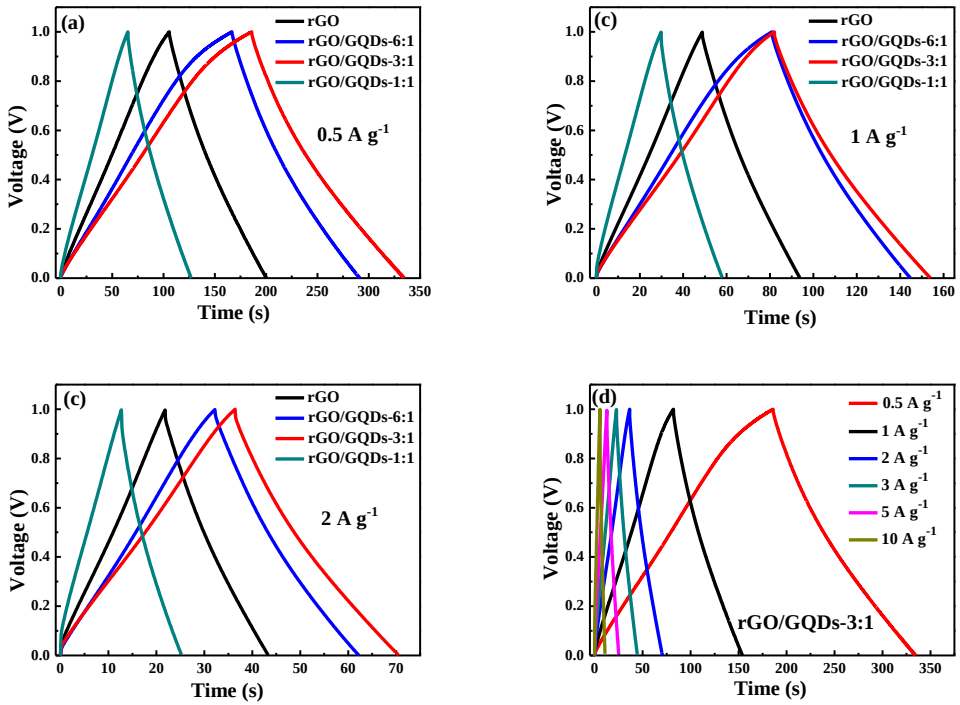


**Figure 4.** (a)-(c) GCD curves of four electrodes at current densities of 0.5 A $g^{-1}$, 1 A $g^{-1}$, and 2 A $g^{-1}$. (d) GCD curves of rGO/GQDs-3:1 electrode at different current densities in 6 M KOH.

No evident IR drop is observed at the start of all discharge curves, and this observation indicates that all of the devices possess low internal series resistance[23, 52] and efficient stored energy extraction. This finding is also confirmed by the linear and symmetrical charge–discharge curves.[53] These superior electrochemical behaviors can be attributed to a large number of active sites provided by the quantum size of graphene particles with high surface areas, which undoubtedly are favorable for the high capacitance. Moreover, the agglomeration of graphene nanosheets can be effectively inhibited by the introduction of GQDs. GQD-anchored graphene nanosheet structure can shorten the transport pathways for electrons and ions and thus accelerate electrochemical kinetics to enhance the capacity retention of rGO/GQD composites.[54]

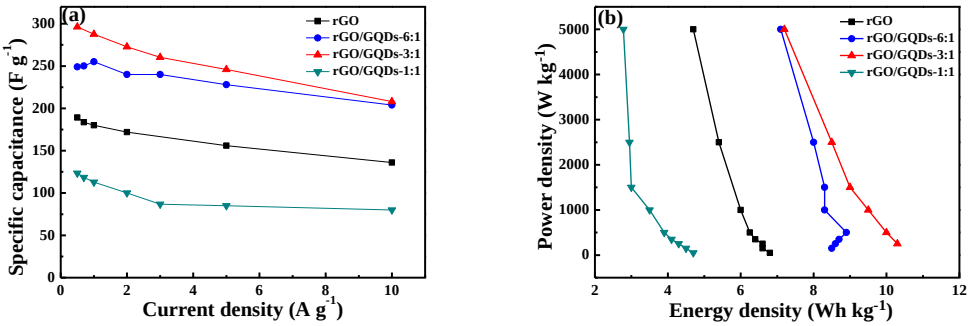


**Figure 5.** (a) specific capacitance of four electrodes at different current densities. (b) Ragone plot of four electrodes in 6 M KOH.

In Fig. 5a, the specific capacitances calculated from the discharge curves ranging from 0.5 A $g^{-1}$ to 10 A $g^{-1}$ of these samples show trends similar to those of the CV curves. The curves also reveal that the highest specific capacitance of 296 F $g^{-1}$ at 0.5 A $g^{-1}$ is observed in rGO/GQD-3:1, and this value is much higher than that of rGO (196 F $g^{-1}$) and rGO/GQD-3:1 (123 F $g^{-1}$) at the same rate. The high discharge capacitance of the rGO/GQD-3:1 electrode may be attributed to the appropriate loading of GQDs on graphene nanosheets. The other reason relies on the fact that ultra-small sized GQDs have larger specific surface area and will bring abundant interfaces into GO/GQDs composites, which can provide more surface area for access of electrolyte ions.[55] At a higher current density, electrolyte ions reach only the exterior surface of electrodes, and the accessible surface area of ions is shortened as the current density increases; as a result, the gravimetric specific capacitance of the samples decreases as the current densities increase.[56] Figure 5b presents the Ragone plot of the samples in 6 M KOH. The maximum energy density and power density of rGO/GQD-3:1 are approximately 10.3 Wh $kg^{-1}$ and 5 kW $kg^{-1}$ according to Eqs. (2) and (3), respectively. This result is in accordance with that shown in Fig. 5a.

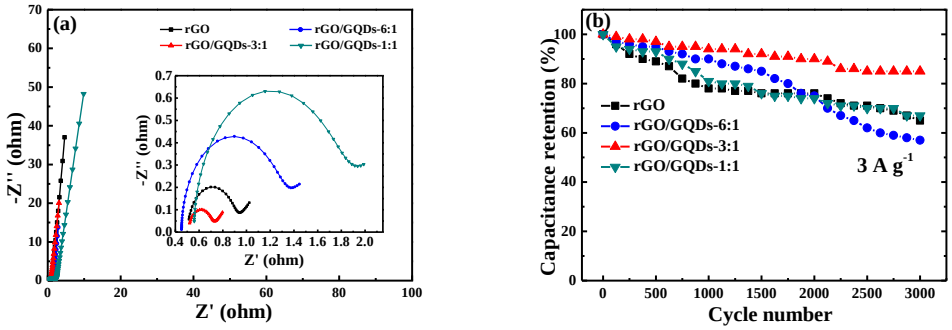


**Figure 6.** (a) Nyquist plots of four electrodes at a frequency rang from 100 mHz to 100 kHz. (b) Cycling stability of four electrodes obtained from GCD curves at 3 A $g^{-1}$ for 3,000 circles.

The formation of micropores in the composite electrodes can also be probed by electrochemical impedance spectroscopy at the open circuit potential in the range of 0.1–100000 Hz. The Nyquist plot of the supercapacitor with four electrodes shows straight lines in the low-frequency region and semicircular patterns in the high frequency region (inset in Fig. 6a). This high frequency loop is related to the electronic resistance between graphene nanosheets.[57] Thus, electrochemical reaction impedance influences the size of semicircles by converting the radius of the smaller semicircle into lower charge transfer resistance.[58] The semicircles of rGO/GQD-3:1 electrode are the smallest among the semicircles in this study, and this observation reveals the low pore-diffusion impedance and charge transfer resistance. The semicircles of rGO/GQD-1:1 electrode is the largest. This finding may be attributed to the formation of GQDs and thus result in the destruction of the graphene matrix and the reduction of electrical conductivity. These results have demonstrated that GQDs can play an active role in improving performance of supercapacitors owing to the conductive GQDs sandwiched between GO nanosheets can facilitate electron transportation from GO to electrolyte, and hence reduce both the internal resistance (Rs) and charge transfer resistance (Rct) of the electrode materials.[55] The

electrode kinetics of GQDs is much slower than that of GO as if the electrode surface is completely blocked mainly because of the increasing number of oxygen-containing groups that prevent electron transfer.[59] The slope of the 45° portion of the curve is called Warburg resistance and is a result of the frequency dependence of ion diffusion in the electrolyte to the electrode interface. The Warburg-type line is short and inclined toward a vertical line, and this characteristic reveals a short ion diffusion pathway and the purely capacitive behavior of rGO/GQD-3:1 electrodes.[60]

The cycling stability and capacitance retention of electrodes are examined by performing a GCD test at 3 A $g^{-1}$ (Fig. 6b). After 3,000 cycles are completed, rGO/GQD-3:1 electrode retains 85% of its initial capacitance, which is higher than those of the other electrodes and indicative of good cycling stability.[61,62]

## 4. CONCLUSION

In summary, binder-free supercapacitors are successfully developed by using GQD-anchored graphene nanosheets. In this structure, GQDs function as a spacer that prevents the restacking of graphene layers. GQD networks in hybrid nanomaterials enhance the accessibility of the charged ions and thus facilitate charge transport and ionic motion during charge/discharge processes in supercapacitors. With the combined advantages of GO and GQDs, the as-prepared rGO/GQD-3:1 composite electrodes yield an excellent gravimetric specific capacitance of 296 F $g^{-1}$ at 0.5 A $g^{-1}$ and retains 85% of their initial capacitance after 3,000 cycles. These values indicate that their electrochemical performance is superior to those of the rGO/GQD-1:1 electrodes. These results suggest that the appropriate mass loading and morphological characteristics of GQDs on graphene nanosheets are important factors to obtain a high capacitance performance. This report presents a simple and easy method to design and synthesize graphene-based composites for high-performance supercapacitor materials and other energy-storage devices. Above all, the advantages induced by incorporation of GQDs into the hybrid electrode materials provides a new pathway to design and synthesis high-performance supercapacitors materials.

ACKNOWLEDGEMENTS
This work was financially supported by National Natural Science Foundation of China (51662004, 11364010, 11304051, 11404072, 11604061, 11664007), Natural Science Foundation of Guangxi Zhuang Autonomous Region of China (2014GXNSFBA118021, 2014GXNSFBA118014, 2015GXNSFBA139002, 2015GXNSFAA139016). Authors acknowledge Prof. Yanwei Li (College of Chemistry and Bioengineering, Guilin University of Technology, Guilin 541004, China.) and Xin Fan (College of Materials Science & Engineering, Guilin University of Technology, Guilin 541004, China.) for experimental help and valuable discussions. Conflict of interests: The authors declare no conflict of interests.

## References

1. Y.W. Li, G.L. Pan, W.Q. Xu, J.H. Yao, L.Z. Zhang, *J. of Power Sources*, 307 (2016) 114-121.

2. J.W. Yang, B. Yan, J. Ye, X. Li, Y.S. Liu, H.P. You, *Phys. Chem. Chem. Phys.*, 16 (2014) 2882-2889.
3. J.W. Yang, B. Yan, J. Ye, X. Li, *Rare Metal Mat. Eng.*, 44(1) (2015) 225-260.
4. Q.Q. Chen, T.T. Zhang, X.C. Qiao, D.Q. Li, J.W. Yang, *J. of Power Sources*, 234 (2013) 197-200.
5. Y.P. Song, H. Wang, Z.H. Li, N.Q. Ye, L.J. Wang, Y. Liu, *RSC Adv.*, 5 (2015) 16386-16393.
6. Y.P. Song, H. Wang, Z.H. Li, N.Q. Ye, L.J. Wang, Y. Liu, *Int. J. Hydrogen Energ.*, 9 (2015) 3613-3623.
7. Y.W. Li, J.H. Yao, Y.X. Zhu, Z.G. Zou, H.B. Wang, *J. of Power Sources*, 203 (2012) 177-183.
8. C. Liu, Z. Yu, D. Neff, A.Zhamu, B.Z. Jang, *Nano Lett.*, 10 (2010) 4863-4868.
9. Y. Wang, Z.Q. Shi, Y. Huang, Y.F. Ma, C.Y. Wang, M.M. Chen, Y.S. CHEN, *J. Mater. Chem. C*, 113 (2009) 13103.
10. W. Yang, M. Ni, X. Ren, Y. Tian, N. Li, Y. Su, X. Zhang, *Curr. Opin. Colloid In.*, 20 (2015) 416-428.
11. Y.W. Zhu, S. Murali, M.D. Stoller, K.J. Ganesh, W.W. Cai, P.J. Ferreira, A. Pirkle, R.M. Wallace, K.A. Cychosz, M. Thommes, D. Su, E.A. Stach, R.S. Ruoff, *Science*, 322 (2011) 1537.
12. C.-M. Chen, Q. Zhang, X.-C. Zhao, B. Zhang, Q.-Q. Kong, M.-G. Yang, Q.-H. Yang, M.-Z. Wang, Y.-G. Yang, R. Schlögl, D.S. Su, *J. Mater. Chem.*, 22 (2012) 14076.
13. Z. Li, P. Qin, L. Wang, C. Yang, Y. Li, Z. Chen, D. Pan, M. Wu, *Electrochim. Acta*, 208 (2016) 260-266.
14. B. Unnikrishnan, C.-W. Wu, I.W.P. Chen, H.-T. Chang, C.-H. Lin, C.-C. Huang, *ACS Sustain. Chem. & Eng.*, 4 (2016) 3008-3016.
15. L. Liu, J. Lang, P. Zhang, B. Hu, X. Yan, *ACS appl. Mater. & interfaces*, 8 (2016) 9335-9344.
16. Y. Huang, J. Liang, Y. Chen, *Small*, 8 (2012) 1805-1834.
17. X. Fan, Z.W. Yang, Z. Liu, *Chinese J. Chem.*, 34(1) (2016) 107-113.
18. X. Fan, Z.W. Yang, Z. Liu, *RSC Adv.*, 5(20) (2015) 15096-15102.
19. Y. Li, G. Louarn, P.-H. Aubert, V. Alain-Rizzo, L. Galmiche, P. Audebert, F. Miomandre, *Carbon*, 105 (2016) 510-520.
20. J. Yan, T. Wei, B. Shao, F. Ma, Z. Fan, M. Zhang, C. Zheng, Y. Shang, W. Qian, F. Wei, *Carbon*, 48 (2010) 1731-1737.
21. S. Chen, J. Zhu, X. Wu, Q. Han, X. Wang, *ACS Nano*, 4 (**2010**) 2822-2829.
22. Y. Zhu, X. Ji, C. Pan, Q. Sun, W. Song, L. Fang, Q. Chen, C.E. Banks, *Energy & Environ. Sci.*, 6 (2013) 3665.
23. R. Li, X. Ren, F. Zhang, C. Du, J. Liu, *Chem. Commun.*, 48 (2012) 5010-5012.
24. Y. Li, H. Zhang, S. Wang, Y. Lin, Y. Chen, Z. Shi, N. Li, W. Wang, Z. Guo, *J. Mater. Chem. A*, 4 (2016) 11247-11255.
25. R. Kumar, A. Agrawal, R.K. Nagarale, A. Sharma, *J. Phys. Chem. C*, 120 (2016) 3107-3116.
26. P. Asen, S. Shahrokhian, *J. Phys. Chem. C*, 121 (2017) 6508.
27. Y.-Q. Dang, S.-Z. Ren, G. Liu, J. Cai, Y. Zhang, J. Qiu, *Nanomaterials*, 6 (2016) 212.
28. F.Y. Shao, M. Li, J.W. Yang, Y.P. Liu, *J. Nano Res-SW*, 30 (2015) 78-85.
29. M. Dinari, M.M. Momeni, M. Goudarzirad, *Surf. Eng.*, 32 (2015) 535-540.
30. J. Luo, H.D. Jang, J. Huang, *ACS Nano*, 7 (2013) 1464-1471.
31. W.-W. Liu, Y.-Q. Feng, X.-B. Yan, J.-T. Chen, Q.-J. Xue, *Adv. Fun. Mater.*, 23 (2013) 4111-4122.
32. A. Ben Gouider Trabelsi, F.V. Kusmartsev, D.M. Forrester, O.E. Kusmartseva, M.B. Gaifullin, P. Cropper, M. Oueslati, *J. Mater. Chem. C*, 4 (2016) 5829-5838.
33. X. Zhou, S. Guo, P. Zhong, Y. Xie, Z. Li, X. Ma, *RSC Adv.*, 6 (2016) 54644-54648.
34. K. Lee, H. Lee, Y. Shin, Y. Yoon, D. Kim, H. Lee, *Nano Energy*, 26 (2016) 746-754.
35. S. Zhang, Y. Li, H. Song, X. Chen, J. Zhou, S. Hong, M. Huang, *Sci. Rep.*, 6 (2016) 19292.
36. W. K. Chee, H. N. Lim, Z. Zainal, N. M. Huang, I. Harrison, and Y. Andou, *J. Phys. Chem. C*, 120 (2016) 4153−4172.
37. Umakant Patil, Su Chan Lee, Sachin Kulkarni, Ji Soo Sohn, Min Sik Nam, Suhyun Han and Seong

Chan Jun, *Nanoscale*, 7 (2015) 6999–7021.
38. Zhibin Lei, Jintao Zhang, Li Li Zhang, Nanjundan Ashok Kumar and X. S. Zhao, *Energy Environ. Sci.*, 9 (2016) 1891-1930.
39. Guanqxun Zhang, Xiao Xiao, Bing Li, Peng Gu, Huaiquo Xue and Huan Pang, *J. Mater. Chem. A*, 5 (2017) 8155-8186.
40. Xu Du, Zhe Zhang, Wei Liu and Yulin Deng, *Nano Energy*, 35 (2017) 299-320.
41. Yongjie Xu, Xinyu Li, Guanghui Hu, Ting Wu, Li Luo, Lang Sun, Tao Tang, Jinfeng Wen, Heng Wang and Ming Li, *Appl. Surf. Sci.*, 422C (2017) 847-855.
42. R. Kumar, R.K. Singh, A.R. Vaz, R. Savu, S.A. Moshkalev, *ACS appl. Mater. & interfaces*, 9 (2017) 8880-8890.
43. S.-Y. Yang, K.-H. Chang, H.-W. Tien, Y.-F. Lee, S.-M. Li, Y.-S. Wang, J.-Y. Wang, C.-C.M. Ma, C.-C. Hu, *J. Mater. Chem.*, 21 (2011) 2374-2380.
44. A.K. Samantara, S. Chandra Sahu, A. Ghosh, B.K. Jena, *J. Mater. Chem. A*, 3 (2015) 16961-16970.
45. X. Li, T. Tang, M. Li, X. He, *J Mater. Sci: Mater. Electron.*, 26 (2015) 1770.
46. X. Li, T. Tang, M. Li, X. He, *Appl. Phys. Lett.*, 106 (2015) 013110.
47. E. Frackowiak, F. Beguin, *Carbon*, 39 (2000) 937-950.
48. Y. Hu, Y. Zhao, G. Lu, N. Chen, Z. Zhang, H. Li, H. Shao, L. Qu, *Nanotechnology*, 24 (2013) 195401.
49. J. Bae, U. Paik, D. Kee Yi, *Mater. Lett.*, 162 (2016) 230-234.
50. V.B. Kumar, A. Borenstein, B. Markovsky, D. Aurbach, A. Gedanken, M. Talianker, Z. Porat, *J. Phys. Chem. C*, 120 (2016) 13406-13413.
51. Y. Li, X. Wang, Q. Yang, M.S. Javed, Q. Liu, W. Xu, C. Hu, D. Wei, *Electrochim. Acta*, 234 (2017) 63-70.
52. J. Shen, A. Liu, Y. Tu, G. Foo, C. Yeo, M.B. Chan-Park, R. Jiang, Y. Chen, *Energy & Environ. Sci.*, 4 (2011) 4220.
53. Q. Chen, Y. Hu, C. Hu, H. Cheng, Z. Zhang, H. Shao, L. Qu, *Phys. Chem. Chem. Phys.*, 16 (2014) 19307-19313.
54. M. Jing, C. Wang, H. Hou, Z. Wu, Y. Zhu, Y. Yang, X. Jia, Y. Zhang, X. Ji, *J. of Power Sources*, 298 (2015) 241-248.
55. X. Zhang, J. Wang, J. Liu, J. Wu, H. Chen, H. Bi, *Carbon*, 115 (2017) 134-146.
56. Y. Huang, A. Gao, X. Song, D. Shu, F. Yi, J. Zhong, R. Zeng, S. Zhao, T. Meng, *ACS appl. Mater. & interfaces*, 8 (2016) 26775-26782.
57. Y. Wang, Z.Q. Shi, Y. Huang, Y.F. Ma, C.Y. Wang, M.M. CHEN, Y.S. CHEN, *J. Phys. Chem. C*, 113 (2009) 13103-13105.
58. X.-D.Z. Li-Feng Chen, Hai-Wei Liang, Mingguang Kong, Qing-Fang Guan, Ping Chen, Zhen-Yu Wu, and Shu-Hong Yu, *ACS Nano*, 6(8) (2012) 7092-7102.
59. X. Jia, X. Ji, *RSC Adv.*, 5 (2015) 107270-107275.
60. S.-M. Li, S.-Y. Yang, Y.-S. Wang, H.-P. Tsai, H.-W. Tien, S.-T. Hsiao, W.-H. Liao, C.-L. Chang, C.-C.M. Ma, C.-C. Hu, *J. of Power Sources*, 278 (2015) 218-229.
61. J.H. Yao, Y.W. Li, Y.X. Li, Y.X. Zhu, H.B. Wang, *J. of Power Sources*, 224 (2013) 236-240.
62. Z.H. Li, H. Wang, Z.Z. Sun, J. Su, Z.Y. Wang, L.J. Wang, *J. Mater. Chem. A*, 4 (2016) 303-313.